Stem Cell Reports
Article

OPEN ACCESS

PI3K/AKT/mTOR Signaling Mediates Valproic Acid-Induced Neuronal Differentiation of Neural Stem Cells through Epigenetic Modifications

Xi Zhang,[1,2,7] Xiaosong He,[1,2,7] Qingqing Li,[1,2,7] Xuejian Kong,[1,2] Zhenri Ou,[1,2] Le Zhang,[1,2] Zhuo Gong,[1,2] Dahong Long,[1,2] Jianhua Li,[3] Meng Zhang,[4] Weidong Ji,[5] Wenjuan Zhang,[6] Liping Xu,[1,2] and Aiguo Xuan[1,2,*]

[1]Key Laboratory of Neuroscience, Key Laboratory of Protein Modification and Degradation, Department of Anatomy, School of Basic Medical Sciences, Guangzhou Medical University, Guangzhou 511436, China
[2]Department of Neurology, Institute of Neuroscience, The Second Affiliated Hospital of Guangzhou Medical University, Key Laboratory of Neurogenetics and Channelopathies of Guangdong Province and the Ministry of Education of China, Guangzhou 510260, China
[3]Department of Physiology, School of Basic Medical Sciences, Guangzhou Medical University, Guangzhou 511436, China
[4]Department of Physiology, Augusta University, Augusta 30912, USA
[5]The First Affiliated Hospital, Center for Translational Medicine, Sun Yat-sen University, Guangzhou 510080, China
[6]Department of Preventive Medicine, School of Medicine, Jinan University, Guangzhou, 510632, China
[7]Co-first author
*Correspondence: xag2005@sohu.com
http://dx.doi.org/10.1016/j.stemcr.2017.04.006

SUMMARY

Although valproic acid (VPA), has been shown to induce neuronal differentiation of neural stem cells (NSCs), the underlying mechanisms remain poorly understood. Here we investigated if and how mammalian target of rapamycin (mTOR) signaling is involved in the neuronal differentiation of VPA-induced NSCs. Our data demonstrated that mTOR activation not only promoted but also was necessary for the neuronal differentiation of NSCs induced by VPA. We further found that inhibition of mTOR signaling blocked demethylation of neuron-specific gene neurogenin 1 (*Ngn1*) regulatory element in induced cells. These are correlated with the significant alterations of passive DNA demethylation and the active DNA demethylation pathway in the *Ngn1* promoter, but not the suppression of lysine-specific histone methylation and acetylation in the promoter region of *Ngn1*. These findings highlight a potentially important role for mTOR signaling, by working together with DNA demethylation, to influence the fate of NSCs via regulating the expression of *Ngn1* in VPA-induced neuronal differentiation of NSCs.

INTRODUCTION

Neural stem cells (NSCs) can differentiate into functional neurons and glial cells (e.g., astrocytes and oligodendrocytes) in the mammalian CNS, which holds powerful potential for regenerative medicine in producing patient-specific cells. This neuronal replacement therapy is based on the idea that neurological functions lost might be recovered by introducing new cells that can differentiate and integrate appropriately to replace the functions of the lost neurons (Carabalona et al., 2016). However, the underlying molecular mechanisms for their fate specification remain ill defined. Accumulating evidence has confirmed that the differentiation of NSCs is regulated by various intrinsic and extrinsic factors (Toma et al., 2014).

The mammalian target of rapamycin (mTOR) is a serine/threonine kinase of the phosphoinositide 3-kinase (PI3K)-related kinases and the catalytic subunit of two distinct complexes called mammalian target of rapamycin complex 1 (mTORC1) and mTORC2. Activation of AKT can be initiated by phosphatidylinositol 3-OH kinase (PI3K), which in turn activates mTORC1 and further downstream targets such as p70S6 kinase. This leads to stimulation of gene transcription, protein synthesis (Parker et al., 2015). mTOR kinase is also a key regulator of the homeostasis of several stem cell pools in which it finely regulates the balance between self-renewal and differentiation in stem cells. Several studies have shown that mTOR activation causes enhanced generation of NSCs/neural progenitor cells, followed by neuronal differentiation (Endo et al., 2009; Marfia et al., 2011), and the inhibition of mTOR abrogates the increase of differentiated neurons (Han et al., 2008). In the CNS the mTOR pathway is also involved in axon regeneration, neuronal activity, and dendritic arborization (Li et al., 2016). Even though the important roles of mTOR in regulating differentiation and development are known, the profound target of mTOR undertaking this process is remained to be addressed.

The transcriptional regulation of cell-type-specific gene expression involves complicated epigenetic events such as DNA demethylation, histone modifications, and chromatin remodeling. DNA methylation/hydroxymethylation influence different stages of NSC differentiation and have been implicated in neural development and differentiation (Kim et al., 2014). The deletion of DNMT1/3b in neuronal progenitor cells results in DNA hypomethylation and triggers astrocyte and early neuronal differentiations, respectively (Fan et al., 2005; Martins-Taylor et al., 2012). In DNMT3a-null mice, impaired post-natal neurogenesis is seen in both the subventricular zone and subgranular zone (Wu et al., 2010). Moreover, DNA methylation can also be catalyzed by TET enzymes such

as TET1, TET2, and TET3 that revert the methylation status of DNA by successive oxidation of 5-methylcytosine (5-mC) into 5-hydroxymethylcytosine (5-hmC), 5-carboxycytosine, and 5-formylcytosine, which are intermediates of an active DNA demethylation mechanism (Hu et al., 2015). Loss of TET1 results in a 45% decrease of NSCs in the subgranular zone, and the neurosphere derived from TET1$^{-/-}$ mice shows impaired growth function (Zhang et al., 2013). However, overexpression of TET2 and TET3 increases 5-hmC formation and leads to defects in neuronal differentiation (Hahn et al., 2013). Furthermore, DNA methylation/demethylation is often found to be coupled with histone modifications during neural development. The upregulation of H3K9 acetylation enhances neural differentiation and activates multiple neurodevelopmental genes (Qiao et al., 2015). However, decreased H3K9 trimethylation severely impairs early neurogenesis and enhances astrocyte formation (Tan et al., 2012). Pro-neural and terminal neuronal genes are poised in stem/progenitor cells by the balance between a repressor histone modification (H3K27me3) and an activator modification (H3K4me3) (McGann et al., 2014). Inhibition of histone deacetylase (HDAC) induces neuronal differentiation of adult NSCs, which is likely mediated through upregulation of neuronal-specific genes, such as neurogenic basic-helix-loop-helix transcription factors *NeuroD*, *Ngn1*, and *Math1* (Hsieh et al., 2004; Yu et al., 2009).

Valproic acid (VPA) is a short-chain carboxylic acid commonly used for the treatment of epilepsy and bipolar disorders. Its pharmacological effects involve distinct mechanisms that affect the transmission of nerve signals in vitro and in vivo. Several intracellular pathways, such as the mTOR pathway, are affected by VPA. VPA activates mTOR signaling in the prefrontal cortex and hippocampus of autistic model rats, characterized by enhanced phospho-mTOR and phospho-S6 (Qin et al., 2016). VPA activates the PI3K/AKT/mTOR pathway in muscle, neuron, and induced pluripotent stem cells (Gurpur et al., 2009; Teng et al., 2014). VPA could also suppress the AKT/mTOR pathway in prostate cancer cells and postmortem fusiform gyrus (Nicolini et al., 2015; Xia et al., 2016). Some recent studies have shown that VPA reduces HDAC activity and promotes neuronal differentiation of NSCs (Hsieh et al., 2004). However, the underlying mechanisms are not fully understood.

Although both mTOR signaling and epigenetic regulation are essential for the differentiation of NSCs in developing or adult brains, a direct connection between mTOR signaling and epigenetic modifications remains uncharacterized in NSCs. In this study, we have set out to determine whether such a link exists, and, if so, how it might impact neural differentiation of VPA-induced NSCs.

RESULTS

Activation of mTOR Signaling Is Required for VPA-Induced Neuronal Differentiation of NSCs

To evaluate the function of mTOR signaling in VPA-induced neural differentiation, we examined the effects of mTOR inhibition and overexpression on neural differentiation, following VPA exposure. We found that VPA treatment caused neuronal differentiation of NSCs (Figure 1A). Interestingly, pretreatment of NSCs with the mTOR-specific inhibitor, rapamycin, remarkably attenuated NSCs from VPA-induced neuronal differentiation (Figure 1A). To further confirm the prodifferentiation role of mTOR, we expressed constitutively active (CA)-mTOR activator Rheb in NSCs and found that mTOR overexpression sensitized NSCs to VPA-induced neuronal differentiation (Figures 1B and 1C). These results suggest that mTOR signaling is critical for VPA-induced neuronal differentiation.

It has been well established that HDAC inhibitors decrease the proliferation of NSCs (Dozawa et al., 2014). We further determined whether the mTOR pathway mediated the effect of VPA on the proliferation of NSCs. We found that rapamycin increased the percentage of bromodeoxyuridine (BrdU)-positive cells and obviously prevented the decrease of VPA-induced proliferation of NSCs. A total of 17% of the cells in VPA-treated cultures were BrdU positive, compared with 47% of the cells in control cultures (Figure 1D). Unexpectedly, rapamycin dramatically enhanced NSCs proliferation (from 17% in VPA-treated cultures to 38% in rapamycin-treated cultures). There was no significant difference in NSC viability among three groups.

VPA Activates the AKT/mTOR/p70S6K Pathway

Previous studies have demonstrated that VPA activates the PI3K/AKT/mTOR pathway in muscle (Gurpur et al., 2009). However, the signaling pathway by which VPA induces neuronal differentiation of NSCs is not clear. To determine the mechanism by which VPA promotes neuronal differentiation, the AKT/mTOR/p70S6K pathway was tested. NSCs treated with VPA for 48 or 72 hr had higher levels of activated AKT, mTOR, and p70S6K (Figure 2A). Immunofluorescence observation revealed that VPA activated p70S6K, and that rapamycin attenuated the expression promoted by VPA (Figure 2B), confirming that VPA activates AKT/mTOR/p70S6K in NSCs.

To determine whether this AKT activation and its resulting downstream effects are triggered by VPA at a shorter time after exposure, 1-day-old differentiating cultures were treated with various concentrations of VPA for 1 hr, extracted, and immunoblotted for total and phosphorylated AKT. Treatment of NSCs with VPA activated AKT within 1 hr. Activation of AKT exhibited a dose-dependent response to VPA (Figure 2C).

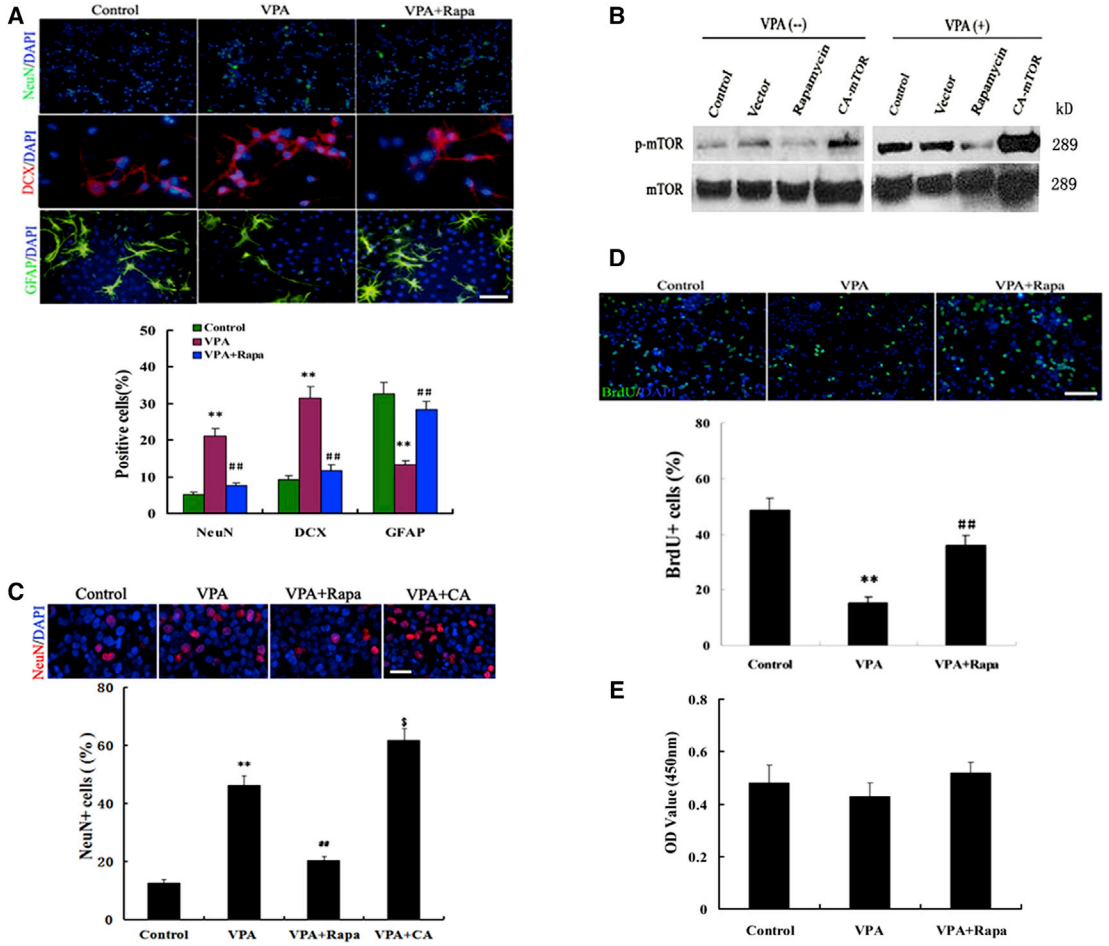

Figure 1. mTOR Activity Is Necessary for Neuronal Differentiation of NSCs Treated with VPA

(A) Immunofluorescence staining and quantification for NeuN, DCX, and GFAP on NSCs. Scale bar, 200 μm. **p = 0.005, 0.002, 0.004 < 0.01 compared with control; ##p = 0.006, 0.002, 0.007 < 0.01 compared with VPA. Data are from three independent experiments.

(B) Western blots of total proteins extracted from NSCs using lentiviral mTOR. The specific protein probed was mTOR and its phosphorylated form. Representative western blot of three independent experiments.

(C) Representative NSCs induced by VPA plus mTOR or VPA. Scale bar, 100 μm. **p = 0.001 < 0.01 compared with control; ##p = 0.008 < 0.01 compared with control; $p = 0.03 < 0.05 compared with VPA. Data are from three independent experiments.

(D) Quantification of proliferation in HDAC inhibitor-treated cultures with or without rapamycin (Rapa). Scale bar, 250 μm. Data are from three independent experiments.

(E) Quantification of viability was assessed by CCK-8 assay. **p = 0.001 < 0.01 compared with control; ##p = 0.04 < 0.01 compared with VPA. One-way ANOVA and Student's t test were used to determine the statistical significance. Data are from four independent experiments.

AKT Activation by VPA Is Dependent on PI3K

Since VPA has HDAC inhibitor activity, kinases expressed or activated as a result of gene modulation may activate AKT independently of PI3K. Alternatively, VPA may activate AKT through the classical PI3K pathway. To differentiate between these possibilities, 1 mmol/L VPA was added on day 2 of differentiation either with or without 100 nmol/L wortmannin, a potent inhibitor of PI3K. Fresh VPA and wortmannin were added every 24 hr thereafter. Microscopic observations revealed that wortmannin attenuated neuronal differentiation of NSCs promoted by VPA (Figure 2D). Immunofluorescence and western blots of extracts made 48 hr after drug exposure demonstrated that wortmannin attenuated the activation of AKT by VPA, confirming that VPA activates AKT through PI3K (Figures 2E and 2F). To exclude the non-specificity of wortmannin on PI3K, the data from knockdown PI3K p110α or p110β were consistent with our above results (Figure S1).

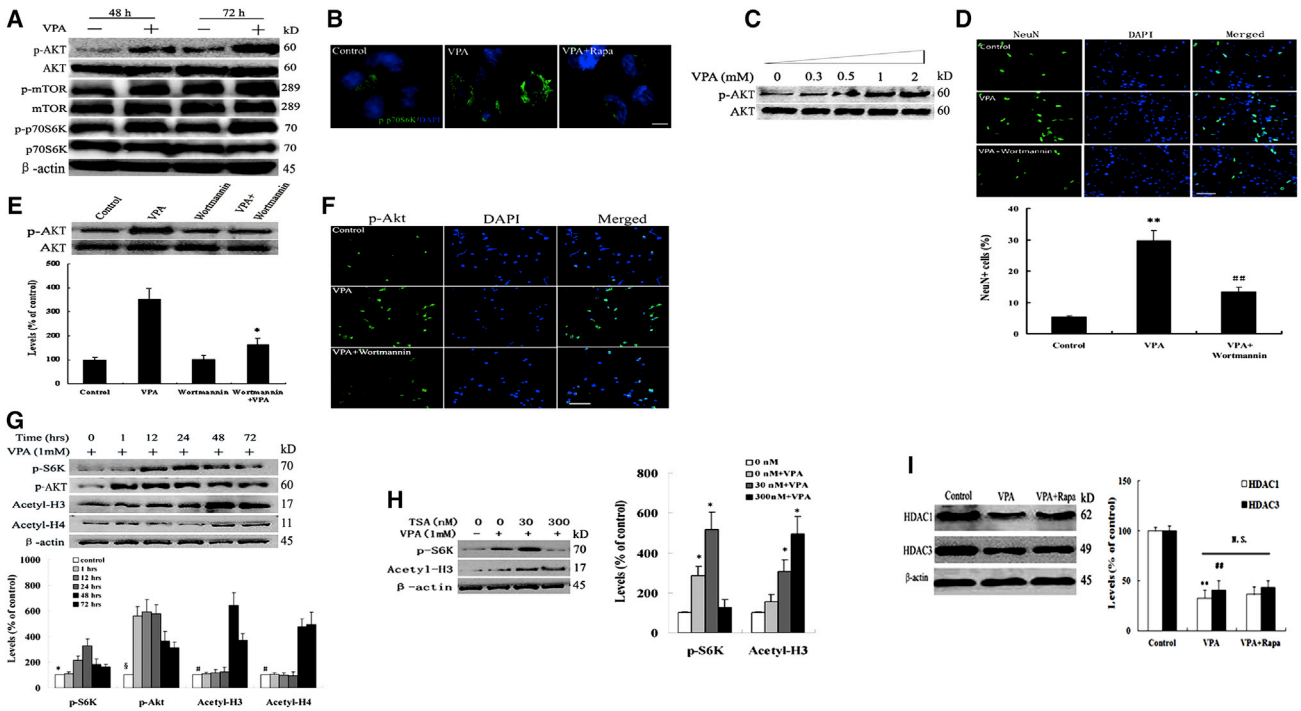

Figure 2. VPA Activates the AKT/mTOR/p70S6K Pathway through a PI3K-Dependent but Not a Histone Acetylation-Dependent Manner in NSCs

(A) VPA (1 mmol/L) was added to duplicate cultures of NSCs for 48 or 72 hr, followed by western blotting using antibodies against the signaling proteins. Higher levels of activated AKT, mTOR, and p70S6K were detected in the VPA-treated NSCs. Representative western blot of three independent experiments.

(B) Immunofluorescence staining for p-p70S6K on NSCs. Higher expression was observed at 1 mmol/L VPA. Scale bar, 50 μm. Representative graph of three independent experiments.

(C) NSCs were exposed to various concentrations of VPA for 1 hr, followed by extraction and western blotting for AKT. VPA activates AKT in a dose-dependent manner, with highest activation seen at 1 mmol/L VPA. Representative western blot of three independent experiments.

(D) NSCs were treated for 48 hr with 1 mmol/L VPA with or without 100 nmol/L wortmannin. Immunofluorescence staining for NeuN showed that the prodifferentiation effect of VPA on NSCs was attenuated by wortmannin. Scale bar, 250 μm, indicating that VPA depends on PI3K for this effect. $^{**}p = 0.001 < 0.01$ compared with control; $^{\#\#}p = 0.006 < 0.01$ compared with VPA. Data are from three independent experiments.

(E) NSCs treated as above were extracted and immunoblotted for phosphor AKT (p-AKT) and total AKT. Ratios of p-AKT to total AKT band intensities were plotted. The AKT-activating effect of VPA was attenuated by wortmannin. $^{*}p = 0.02 < 0.05$ compared with VPA. Data are from three independent experiments.

(F) Immunofluorescence staining for p-AKT on NSCs. Wortmannin decreased the expression of p-AKT induced by VPA. Scale bar, 250 μm. Representative graph of three independent experiments.

(G) VPA activated AKT/p70S6K signaling and enhanced histone H3 and H4 acetylation. NSCs were stimulated with 1 mM of VPA for various times and the levels of p-AKT, phospho-p70S6K, acetyl-H3, and acetyl-H4 were analyzed by immunoblotting. Both AKT and S6K proteins activation preceded the onset of histone H3 and H4 acetylation. $^{*}p = 0.03, 0.01 < 0.05$ compared with 12 and 24 hr; $^{\S}p = 0.007, 0.005, 0.007, 0.01, 0.03 < 0.05$ compared with 1, 12, 24, 48, and 72 hr; $^{\#}p = 0.008, 0.02, 0.01, 0.01 < 0.05$ compared with 48 and 72 hr. Data are from three independent experiments.

(H) The effects of VPA and TSA on acetyl-H3 accumulation appeared to be additive. TSA alone appeared to elevate levels of phospho-p70S6K, but the increases were not concentration dependent. A higher concentration of TSA (300 nM) attenuated VPA-induced increases in phospho-p70S6K. $^{*}p = 0.03, 0.006, 0.02, 0.008 < 0.05$ compared with control. Data are from three independent experiments.

(I) NSCs were treated by VPA or VPA plus rapamycin. Lysates from the cells were analyzed by immunoblotting for the levels of HDAC1, HDAC3, and β-actin. Rapamycin (Rapa) increased HDAC1 and HDAC3 levels but did not significantly alter the magnitude of VPA-induced decreases in HDAC1 and HDAC3 levels. $^{**}p = 0.006 < 0.01$ compared with control; $^{\#\#}p = 0.008 < 0.01$ compared with control. One-way ANOVA and Student's t test were used to determine the statistical significance. Data are from three independent experiments.

AKT Activation by VPA Is Independent on Histone Acetylation

VPA rapidly and concentration-dependently induces accumulation of acetylated H3 and H4 (Godino et al., 2015). To exclude the possibility that AKT activation may be triggered by histone modification, we tested the effects of VPA on phosphorylation of AKT, S6K, and acetylation of histone H3 and H4. Our results showed that VPA activated S6K from 12 hr and reached a plateau at 24 hr. VPA activated AKT from 1 hr and reached a plateau at 12 hr, which preceded the increase of S6K phosphorylation. In addition, both AKT and S6K protein activation also preceded the onset of histone H3 and H4 acetylation (Figure 2G). Moreover, trichostatin A (TSA), a potent HDAC inhibitor, concentration-dependently induced accumulation of acetylated H3. TSA at a low concentration induced a significant increase in phospho-S6K levels, yet this increase plateaued at a higher TSA concentration (Figure 2H). These data indicate that TSA produces a limited effect on the mTOR pathway that does not parallel its effect on acetyl-H3 accumulation (Figure 2H). TSA at a low concentration induced additive effects on VPA-induced acetyl-H3 accumulation, but not on VPA-induced increases in phosph-S6K levels. TSA at a high concentration significantly attenuated VPA-induced increases in phospho-S6K levels. These results suggest that VPA-induced AKT activation is independent on its effect on histone modification.

Although both AKT and S6K protein activation preceded the onset of histone acetylation, to exclude the possibility that AKT/mTOR/p70S6K signaling activation in turn promotes histone acetylation, we investigated the effects of VPA with or without rapamycin on expression of HDACs. Unexpectedly, we observed that rapamycin increased HDAC1 and HDAC3 levels, but did not significantly alter the magnitude of VPA-induced decreases in HDAC1 and HDAC3 levels (Figure 2I). This finding indicates that AKT/mTOR/p70S6K signaling may not direct the histone acetylation.

PI3K/AKT/mTOR Activity Regulated Passive DNA Demethylation during Differentiation Induced by VPA

DNA methylation/demethylation are essential epigenetic modifications controlling gene expression during differentiation and development (Orlanski et al., 2016). Since the inhibitors of histone deacetylation cause epigenetic DNA modifications, we next further evaluated whether PI3K/AKT/mTOR activity regulates VPA-induced neuronal differentiation by repressing DNA methylation. We found that the mRNA expression profiles of passive DNA demethylation pathway enzymes DNMT1, DNMT3a, but not DNMT3b and DNMT3L, were significantly decreased in NSCs treated with 1 mM VPA for 1 day (Figure 3A). Similar results were obtained from the protein blot experiments (Figure 3B). Surprisingly, PI3K/AKT/mTOR inhibition markedly attenuated the decreases in the passive DNA demethylation pathway enzymes (Figures 3A and 3B). Interestingly, we also found that the expression of the neuron-specific gene *Ngn1* was much greater in VPA-treated cells than in the DMSO-treated controls, and that its expression was also affected by PI3K/AKT/mTOR inhibition (Figures 3A and 3B). Our results suggested that PI3K/AKT/mTOR activity may stimulate the activation of *Ngn1* through suppressing the expression of DNMT 1 and 3a, which triggered VPA-induced neural differentiation of NSCs.

To clarify whether the increased expression of *Ngn1* induced by VPA is a direct result of inhibiting the putative DNMTs, we studied the effects of VPA on the genome-wide DNA demethylation and gene-specific promoter demethylation. In the control group, 5-mC immunostaining (im) was highly intense and distributed throughout the nucleus (Figure 3C). However, in the VPA-treated group, decreased 5-mC-im intensity was seen in the nucleus, but preferentially distributed near the nuclear membrane into differentiation (Figure 3C). We next examined the effect of PI3K/AKT/mTOR inhibition on genome-wide DNA methylation. As expected, rapamycin obviously attenuated the decreased 5-mC-im intensity induced by VPA (Figure 3C), suggesting an important role for mTOR signaling in VPA-induced DNA demethylation, which resulted in Ngn1 expression. This notion was further confirmed by dot blotting for 5-mC (Figure 3D). As *Ngn1* expression is known to be repressed by methylation of CpG dinucleotides within its promoter, We next further examined the effect of VPA on gene-specific promoter demethylation; bisulfite sequence analysis revealed that NSCs treated with VPA showed nearly 40% loss of 5-mC in the *Ngn1* promoter region between −171 and 140 than that of control NSCs (Figure 3E). Furthermore, rapamycin treatment showed 20% gain of 5-mC in the same region (Figure 3E). DNA methylation levels of the *Ngn1* promoter region in rapamycin-treated cells with or without VPA were further verified by EpiMark 5-mC Analysis Kit (Figure 3F). Taken together, our findings indicate that mTOR inhibition mostly blocks the DNA demethylation of neuronal target gene caused by VPA during differentiation.

PI3K/AKT/mTOR Activity Facilitates TET-Mediated DNA Hydroxymethylation during VPA-Induced Differentiation

DNA demethylation involves passive and active demethylation. By converting 5-mC to 5-hmC following the base excision repair pathway, TET family proteins were shown to promote active DNA demethylation in mammalian cells (Kafer et al., 2016). We next focused our investigation on the genes mediating active demethylation. We found upregulation of

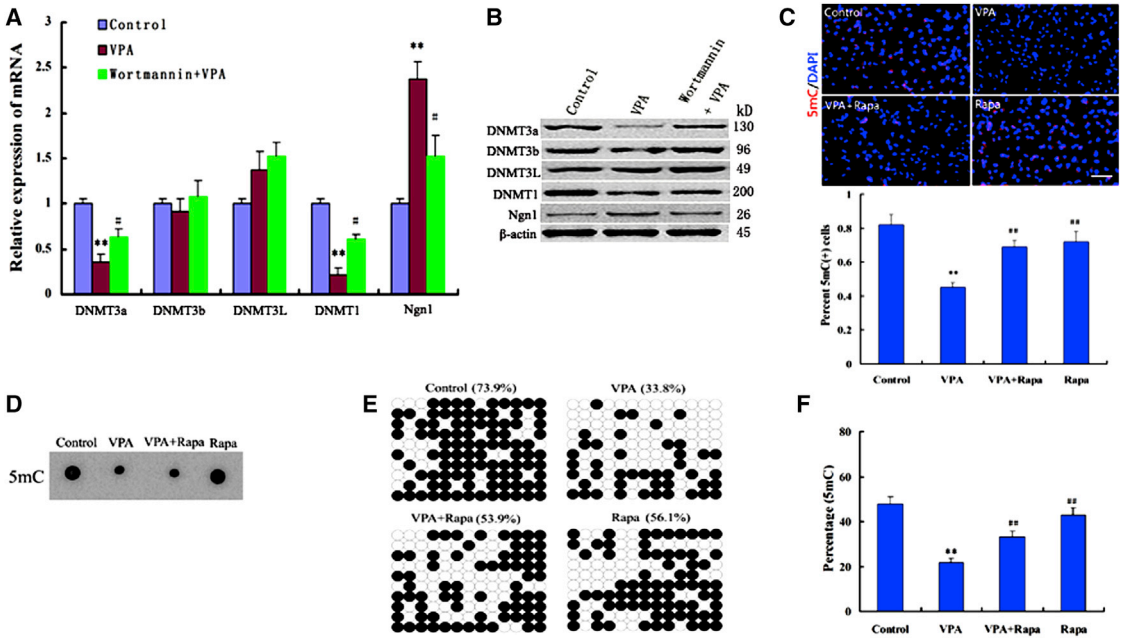

Figure 3. PI3K/AKT/mTOR Activity Regulates Passive DNA Demethylation during VPA-Induced Differentiation

(A and B) Relative levels of mRNA and protein for different Dnmts and *Ngn1* in NSCs treated with either VPA or VPA plus wortmannin. Results were normalized with β-actin. $^{**}p = 0.006$, $0.004 < 0.01$ compared with control; $^{\#}p = 0.04$, $0.03 < 0.05$ compared with VPA. Data are from three independent experiments.

(C) Immunofluorescence staining for 5-mC showed that the intensity of VPA on 5-mC-immunostaining was attenuated by rapamycin (Rapa). Scale bar, 250 μm. $^{**}p = 0.002 < 0.01$ compared with control; $^{\#\#}p = 0.006$, $0.004 < 0.01$ compared with VPA. Data are from three independent experiments.

(D) Dot blot analysis of 5-mC quantity during differentiation of NSCs. Dot blot performed by biotinylation of 5-mC followed by probing with Avidin-HRP. Dot blot representative of three independent experiments.

(E) Bisulfite DNA sequencing analysis to part of the *Ngn1* promotor region in NSCs treated with VPA or rapamycin. Filled and open circles represent methylated and unmethylated CpGs, respectively. The percentage of total methylated CpGs for each analyzed region is given on top of each dataset.

(F) Relative quantitation of 5-mC within a specific locus was performed using the EpiMark 5-mC Analysis Kit followed by real-time PCR analysis. $^{**}p = 0.003 < 0.01$ compared with control; $^{\#\#}p = 0.008$, $0.006 < 0.01$ compared with VPA. One-way ANOVA and Student's t test were used to determine the statistical significance. Data are from three independent experiments.

TET1, TET2, and TET3 protein levels in VPA-treated cells, this effect can be inhibited by rapamycin treatment (Figure 4A). However, the small difference in TET1, TET2, or TET3 protein expressions between DMSO- and rapamycin-treated cells showed that the effect of VPA on TETs is dependent on the mTOR signaling in NSCs (Figure 4A). To further confirm the expression of the TET family members in every group, we immunohistochemically evaluated the intensity of the TET family. As expected, the immunohistochemical results were consistent with previous TET protein levels (Figure 4B). TET-im intensity was significantly increased in NSCs subjected to VPA when compared with control (Figure 4B). Furthermore, following rapamycin treatment, TET-im intensity was significantly lower in VPA + rapamycin-treated cells than in VPA-treated cells (Figure 4B).

To further verify the effect of TETs on active DNA demethylation, an anti-5-hmC antibody-based dot blot analysis showed an increase of 5-hmC induced by VPA treatment (Figure 4C). Whereas rapamycin and VPA treatment strongly decreased 5-hmC levels (Figure 4C), consistent with our dot blot results we found that 5-hmC covered an increasing amount of the genome, and 5-hmC-im became more intense in VPA-treated cells, a low density for 5-hmC signature was observed in cells treated by VPA + rapamycin (Figure 4D). To determine if 5-hmC has a functional role in regulating neural differentiation, we calculated enrichment of 5-hmC at the *Ngn1* promotor and found that 5-hmC becomes especially enriched in VPA-treated cells (Figure 4E). We also observed a significant reduced enrichment of 5-hmC at promotor region of Ngn1 in VPA + rapamycin-treated cells (Figure 4E). These results confirmed that the loss of *Ngn1* promoter DNA methylation in NSCs treated with VPA is induced by increased expressions

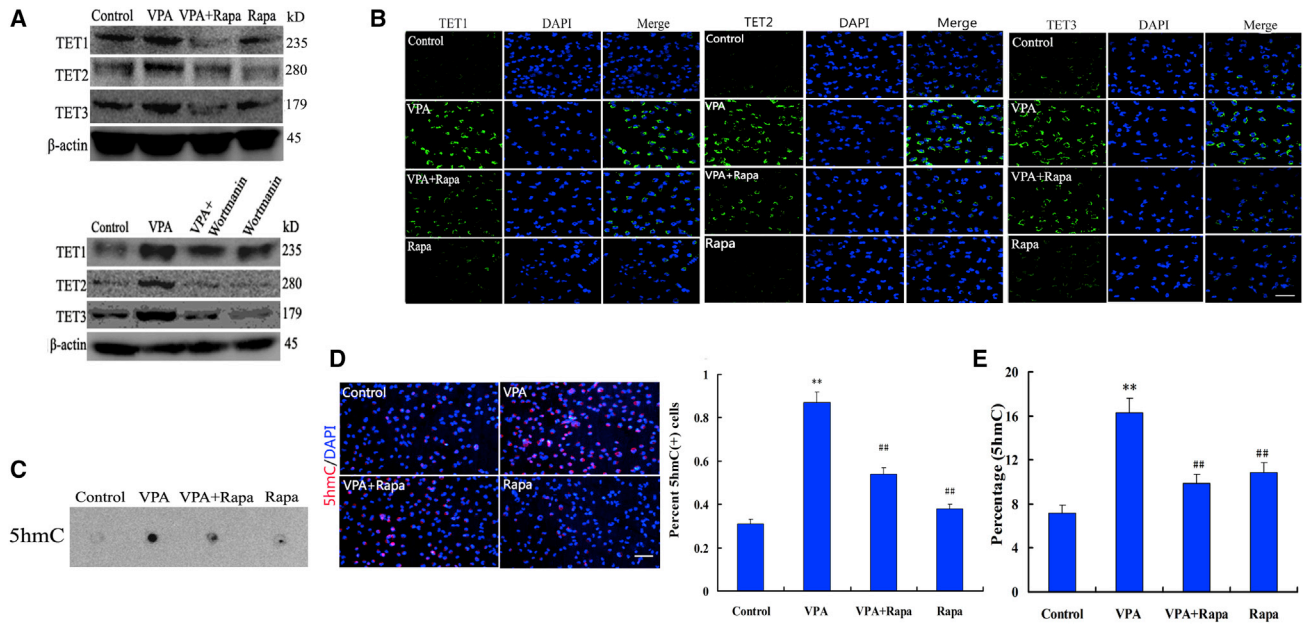

Figure 4. PI3K/AKT/mTOR Activity Promotes DNA Hydroxymethylation during Differentiation Induced by VPA

(A and B) The expression of TET1, TET2, and TET3 proteins was analyzed by immunoblotting and immunofluorescence staining. Scale bar, 250 μm. Representative graphs of three independent experiments.

(C) Dot blot analysis of 5-hmC quantity during differentiation of NSCs. Dot blot performed by biotinylation of 5-hmC followed by probing with Avidin-HRP. Dot blot representative of three independent experiments.

(D) Immunofluorescence staining for 5-hmC showed that the intensity of VPA on 5-hmC-immunostaining was attenuated by rapamycin (Rapa). Scale bar, 250 μm. $^{**}p = 0.001 < 0.01$ compared with control; $^{\#\#}p = 0.005, 0.003 < 0.01$ compared with VPA. Data are from three independent experiments.

(E) Relative quantitation of 5-hmC within a specific locus was performed using EpiMark 5-hmC Analysis Kit followed by real-time PCR analysis. $^{**}p = 0.002 < 0.01$ compared with control; $^{\#\#}p = 0.004, 0.006 < 0.01$ compared with VPA. One-way ANOVA and Student's t test were used to determine the statistical significance. Data are from four independent experiments.

of active DNA demethylation pathway enzymes through activating mTOR signaling.

VPA but Not PI3K/AKT/mTOR Activity Regulates Histone Modifications in the Ngn1 Gene Region

As mentioned above, VPA elevated the *Ngn1* expression in differentiated cells and also regulated the expression of HDACs. To determine whether PI3K/AKT/mTOR signaling mediates VPA-induced *Ngn1* expression via regulating the histone modifications, we employed western blot and chromatin immunoprecipitation (ChIP) assays to test histone acetylation and histone modifications at the proximal promoter of the *Ngn1* gene after VPA treatment. We detected an abundance of acetylated histone H3 and H4 in extracts of cells treated by VPA (Figure 5A). Interestingly, the level of acetylated histone H3 and H4 remained relatively unchanged in extracts of cells treated by VPA + wortmannin compared with VPA (Figure 5A), suggesting that there is less functional relationship between PI3K/AKT/mTOR signaling and histone acetylation during VPA-induced differentiation. To further define the relationship, we investigated histone modifications at the proximal promoter of the *Ngn1* gene after VPA and/or rapamycin treatment. Our data showed that, while trimethylated H3K4 (H3K4me3) significantly increased with VPA treatment at the proximal promoter of the *Ngn1* gene, acetylated H3K9 (H3K9Ac) was also obviously enhanced (Figure 5B). The results suggest that the efficient recruiting of H3K4me3 and H3K9Ac at the promoter is a prerequisite for the activation of the *Ngn1* gene after VPA treatment. We then analyzed the recruiting of methylated lysine in H3K27 and H3K9 on the promoter region of *Ngn1* with ChIP assay. Our observation showed that the cells treated with VPA decreased the trimethylated H3K9 (H3K9me3) and dimethylated H3K9 (H3K9me2) levels in the *Ngn1* promoter (Figure 5B). By contrast, no significant differences in histone modifications were found between VPA-treated and VPA + wortmannin-treated cells (Figure 5B). In addition, western blot analysis was in accordance with the above data (Figure 5C). These findings suggest that VPA but not PI3K/AKT/mTOR activity mediates histone modifications in the *Ngn1* gene region.

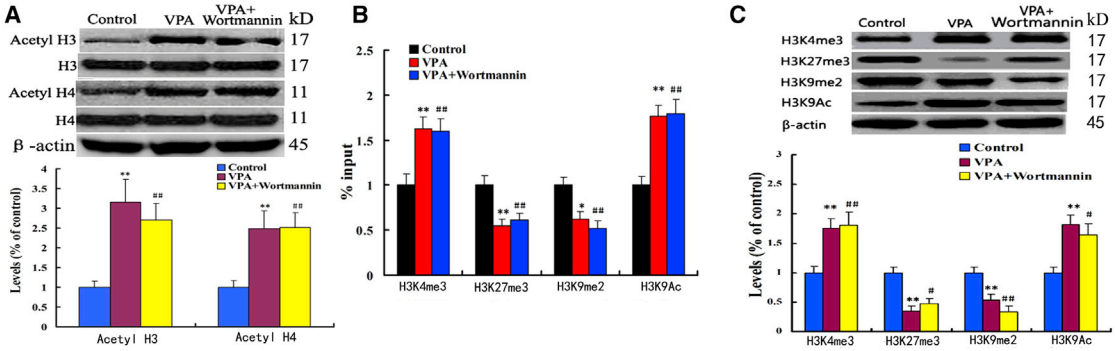

Figure 5. VPA but Not PI3K/AKT/mTOR Activity Regulates Histone Modifications in the *Ngn1* Promotor Region

(A) The levels of histone H3 and H4 acetylation in extracts of NSCs treated by VPA or VPA plus wortmannin. **p = 0.003, 0.006 < 0.01 compared with control; ##p = 0.005, 0.005 < 0.01 compared with control. Data are from three independent experiments.

(B) H3K4me3, H3K27me3, H3K9me2, and H3K9Ac at the Ngn1 promoter were analyzed by ChIP analysis in the NSCs. The acetylation and methylation levels were expressed as the ratio of the signal intensity of the immunoprecipitation product to the input. **p = 0.005, 0.008, 0.003 < 0.01 compared with control; *p = 0.02 < 0.05 compared with control; ##p = 0.006, 0.009, 0.007, 0.003 < 0.01 compared with control. Data are from three independent experiments.

(C) NSCs were treated by VPA or VPA plus wortmannin, followed by western blotting using antibodies against H3K4me3, H3K27me3, H3K9me2, and H3K9Ac. **p = 0.005, 0.004, 0.007, 0.004 < 0.01 compared with control; #p = 0.03, 0.02 < 0.05 compared with control; ##p = 0.004, 0.003 < 0.01 compared with control. Data are from three independent experiments.

DNMTs Inhibitor Rescues the Differentiation Arrested by PI3K/AKT/mTOR Inhibition or VPA Deprivation

To address whether the elevated expression of DNMT1 and 3a represents a significant cause for the differentiation arrested by loss of PI3K/AKT/mTOR activity or VPA deprivation, we applied the DNMT inhibitor, 5-aza-2′-deoxycytidine (AZA), to the culture medium. AZA is a cytidine analog that blocks actions of DNMTs and causes passive demethylation. Treatment with AZA in the presence of VPA + PI3K/AKT/mTOR inhibition resulted in a 1.7-fold increase in the number of neuronal nuclei (NeuN)-positive cells, compared with VPA + wortmannin treatment control (Figure 6A). Upon removing VPA and wortmannin, we could still observe a significant 2.2-fold in NeuN-positive cells from AZA-treated cells compared with control (Figure 6A). Immunohistochemical staining for doublecortin (DCX) and western blot further confirmed these data (Figures 6A and 6B). These results indicated that inhibition of DNMT1 and 3a significantly rescues the trapped differentiation by PI3K/AKT/mTOR inhibition or VPA deprivation.

TET1, TET2, and TET3 Are Necessary for the Neuronal Differentiation of NSCs Induced by VPA

To explore whether the activity of TETs is required for VPA-induced neuronal differentiation, loss of function of TETs were testified. We found that expression of TET1, TET2, and TET3 proteins was efficiently downregulated by shTET1, shTET12, and shTET13 treatments (Figure 7A), along with a reduction of 5-hmC protein as well as an increment of 5-mC protein- compared with VPA-treated cells (Figures 7B and 7C). The knockdown of TET1, TET2, and TET3 markedly abolished VPA-mediated increase of DCX + neuron yields (Figure 7D) and *Ngn1* protein expressions (Figure 7E). Furthermore, shTET1, shTET12, and shTET13 treatments in VPA-treated cultures led to a robust reduction of 5-hmC enrichment and increase of 5-mC in the *Ngn1* gene promoter (Figures 7F and 7G). These findings suggested that VPA-induced neuron differentiation is dependent on TETs-mediated DNA hydroxymethylation/demethylation.

DISCUSSION

Some recent studies have shown that activation of the mTOR pathway participates in the neuronal differentiation regulation of mouse olfactory bulb stem cells and neural progenitor cells (Han et al., 2008; Otaegi et al., 2006). We demonstrated here that VPA activated mTOR signaling and elevated mTOR activity, significantly enhancing VPA-induced neuronal differentiation of NSCs. VPA-induced differentiation was suppressed by the mTOR inhibitor, rapamycin, indicating activation of the mTOR pathway in differentiation induced by VPA. Immunoblotting with antibodies against activated or total AKT, mTOR, and p70S6K showed that VPA activated this pathway, indicating the effects of VPA on NSCs are mediated, at least in part, by activating the AKT/mTOR/S6K pathway.

Wortmannin is a selective and irreversible inhibitor of PI3K and was used to distinguish whether VPA activated

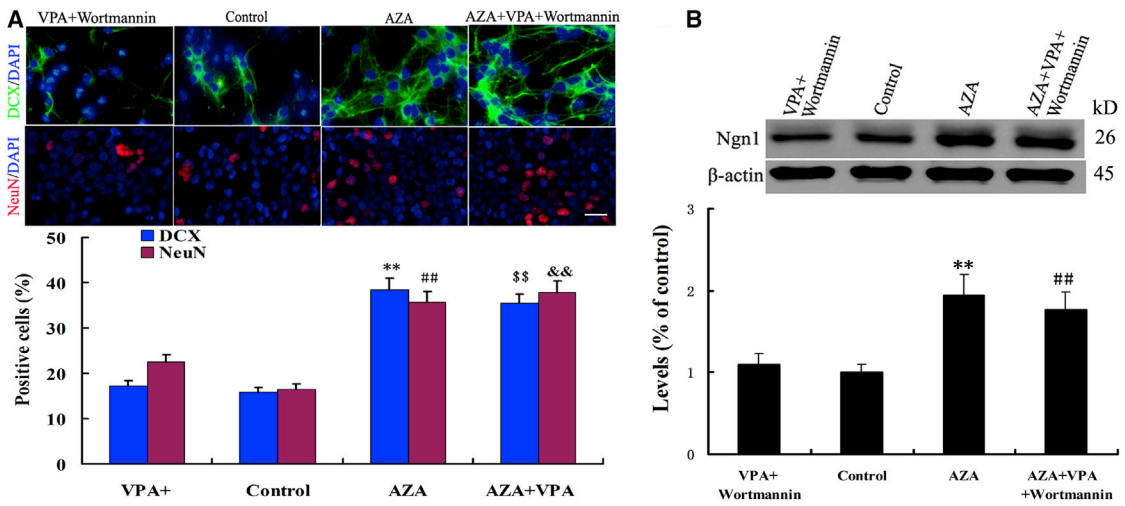

Figure 6. DNMTs Inhibitor Rescues Impeded Differentiation by PI3K/AKT/mTOR Inactivation or VPA Deprivation

(A) Immunofluorescence staining and quantification for NeuN and DCX on NSCs under different treatment conditions. Scale bar, 100 μm. $^{**}p = 0.002 < 0.01$ compared with control; $^{\#\#}p = 0.004 < 0.01$ compared with control; $^{\$\$}p = 0.006 < 0.01$ compared with VPA + wortmannin; $^{\&\&}p = 0.006 < 0.01$ compared with VPA + wortmannin. Data are from three independent experiments.

(B) The expression of *Ngn1* protein was analyzed by immunoblotting in different treatment groups. $^{**}p = 0.004 < 0.01$ compared with control; $^{\#\#}p = 0.006 < 0.01$ compared with VPA + wortmannin. Data are from three independent experiments.

AKT via the classical PI3K pathway or via an alternate pathway. Wortmannin reduced AKT activation by VPA, indicating that AKT activation by VPA is dependent on PI3K. Moreover, wortmannin inhibited the neuronal differentiation promoted by VPA, confirming that PI3K-mediated AKT activation by VPA is necessary to induce neuronal differentiation in NSCs. Because wortmannin is a non-specific inhibitor of PI3K, we also found that PI3K p110α or PI3K p110β knockdown inhibited AKT activation and attenuated the neuronal differentiation of NSCs with VPA, which was consistent with the results of wortmannin. However, the mechanism by which VPA activates the PI3K/AKT pathway is currently unknown but it may be mediated through direct effect of VPA on PI3K.

VPA is an HDAC inhibitor and plays a role in modifying chromatin structure and gene expression. The post translational modifications of the amino-terminal tails of the H3 and H4 histones also involve in general changes in condensation of chromatin connected with various tissue-specific genes, which maintain them in either an activated or repressed state. VPA treatment enhances histone acetylation, but also activates mTOR signaling. HDAC1 and HDAC2 knockdown demonstrated that the interaction with mTOR signaling is initiated by histone H3 acetylation (Makarević et al., 2014). The HDAC inhibition represses cancer proliferation via suppressing PI3K/mTOR pathways (Wilson-Edell et al., 2014). Histone acetylation also increases after rapamycin treatment or siRNA knockdown of mTOR in gastric cancer (Sun et al., 2014). On the basis of our observations that VPA triggered global histone hyperacetylation through suppressing the activity of HDACs and activated PI3K/AKT/mTOR pathway, we raise the hypothesis that VPA may activate PI3K/AKT/mTOR pathway via promoting histone hyperacetylation. However, we failed to obtain conclusive evidence to support the notion that VPA activated the mTOR pathway by inhibiting HDACs. Findings from a recent study showed that H3 and H4 acetylation in the hippocampus depends on ERK activation (Zhao et al., 2010). Our results thus also indicated that mTOR pathway activation did not trigger histone acetylation.

Histone acetylation and DNA methylation operate in a concerted manner. In agreement with this hypothesis, HDAC inhibitors such as MS-275 and TSA also reduce DNMT1, 3a and 3b protein levels and enzyme activity in NT-2 precursor cells, tentatively explaining the mechanism of DNA demethylation (Kundakovic et al., 2009). In cultured NSCs, we found no changes in DNMT3b and DNMT3L levels upon VPA administration. VPA or other HDAC inhibitors induce promoter demethylation by activating DNA demethylation mechanisms (Detich et al., 2003; Guidotti et al., 2011). We discovered that PI3K/AKT/mTOR inhibition enhanced DNMT1 and 3a expression and thus enhanced the stimulation of methylation activity specific for neuronal gene silencing during differentiation. Although there is no direct evidence, our finding that PI3K/AKT/mTOR activity stimulated DNMT1 and 3a expression therefore sheds new light on the role played by VPA signaling for both inhibition of proliferation and differentiation of NSCs. Inhibition of HDAC activity

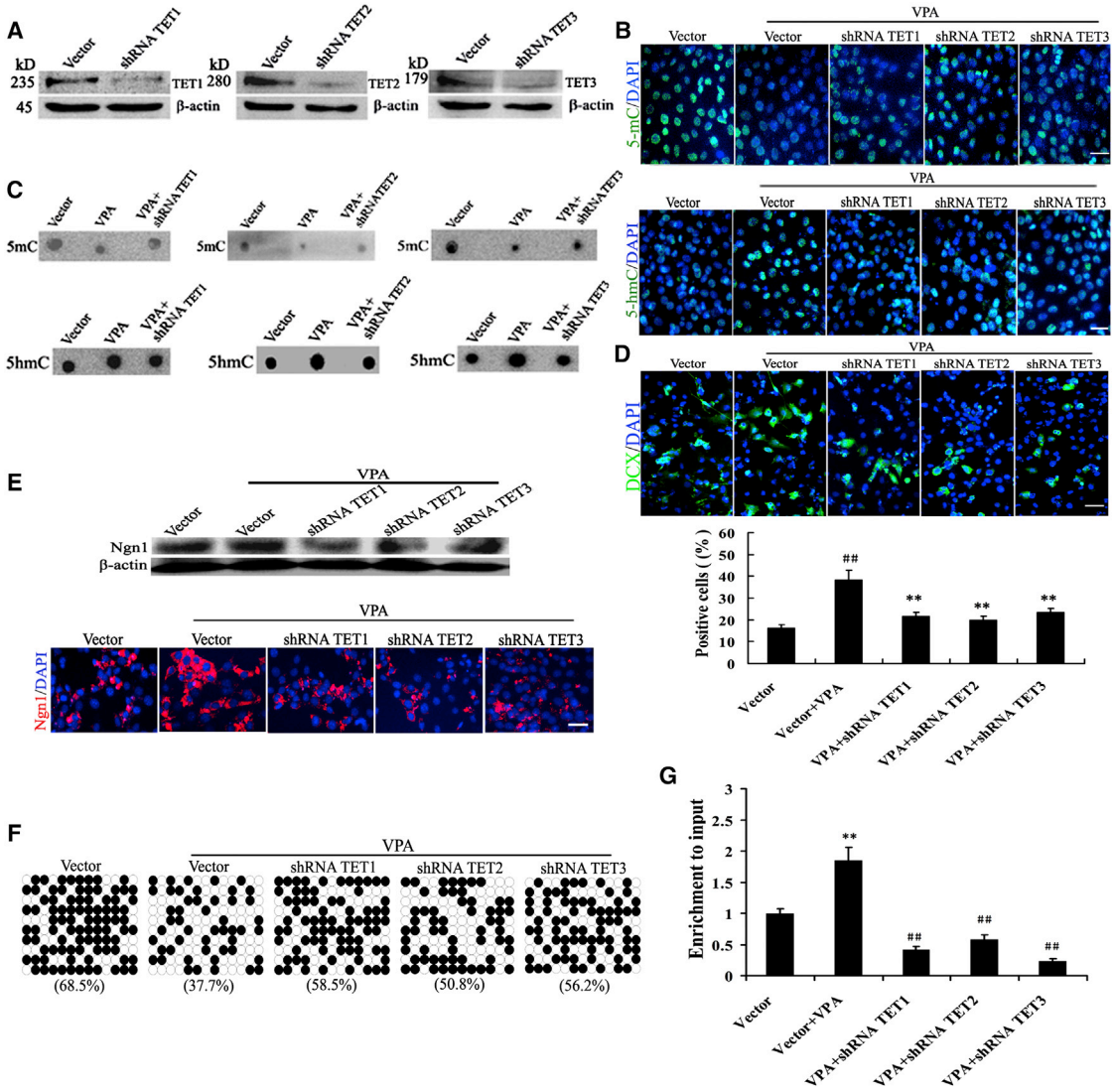

Figure 7. TET1, TET2, and TET3 Are Required for VPA-Induced Neuronal Differentiation of NSCs

(A) NSCs were transfected with TET1, TET2, TET3, or control shRNA for 48 hr. Lysates from the cells were analyzed by immunoblotting for the levels of TET1, TET2, TET3, and β-actin. Immunoblotting representative of three independent experiments.

(B and C) TET1, TET2, or TET3 knockdown suppressed VPA-induced reduction of 5-hmC protein and an increment of 5-mC protein in immunocytochemical (B) and dot blot (C) analyses. Scale bar, 100 μm. Representative graphs of three independent experiments.

(D) TET1, TET2, or TET3 downregulation reversed the neuronal differentiation of VPA-treated NSCs. Scale bar, 100 μm. $^{**}p = 0.004, 0.003, 0.004 < 0.01$ compared with VPA (Vector + VPA); $^{\#\#}p = 0.000 < 0.01$ compared with control (Vector). Data are from three independent experiments.

(E) The expression of *Ngn1* protein was analyzed by immunoblotting and immunocytochemistry. Scale bar, 100 μm. Representative graphs of three independent experiments.

(F) Bisulfite DNA sequencing for DNA methylation status in the *Ngn1* gene regions close to the TSS (−171 to +140 CpGs).

(G) 5-hmC enrichment in the promoter region of the *Ngn1* gene was also assessed by 5-hmC DIP-qPCR analysis. $^{**}p = 0.008 < 0.01$ compared with control; $^{\#\#}p = 0.002, 0.003, 0.000 < 0.01$ compared with VPA. Data are from three independent experiments.

promotes the ubiquitin-dependent proteasomal degradation of DNMT1 (Du et al., 2010), further suggesting a synergistic promotion of DNA demethylation by suppression of DNMTs activities. Furthermore, we also observed that VPA promotes the DNA hypomethylation in mTOR-dependent manner. The fact that mTOR activation is necessary for other protein kinases to decrease gene-specific DNA methylation suggests that mTOR signaling

may critically link cell-signaling mechanisms with DNA methylation.

VPA is a well-known DNA demethylating agent. It can induce passive DNA demethylation by suppressing DNMT1, DNMT3a, and DNMT3b, which triggers the activation of genes (Dong et al., 2010). The evidence we present here thus supports a model where PI3K/AKT/mTOR activation by VPA orchestrates the epigenetic events during differentiation, allowing complete activation of the neuron-specific gene, *Ngn1*. We found that hypermethylation of the *Ngn1* promoter region, as the result of PI3K/AKT/mTOR inhibition, is tightly correlated with the significantly elevated DNMT1 and 3a expression compared with control cells. Accordingly, we demonstrated that inhibiting DNMT activity by AZA significantly enhanced *Ngn1* expression and rescued the differentiation arrested by PI3K/AKT/mTOR inhibition or VPA deprivation. Our data thus strongly argue that PI3K/AKT/mTOR signaling plays a critical function in facilitating the passive demethylation of endogenous global and neuron-specific genes by suppressing the expression of DNMT1 and 3a in cells with VPA.

Active demethylation of DNA is a common mode of epigenetic control of tissue-specific gene expression during development through TET enzymes (Hirabayashi and Gotoh, 2010). DNA 5-hmC, catalyzed by TET enzymes, recently opened up as an important epigenetic signature to control biological activities in developing and adult tissues (Kriaucionis and Heintz, 2009). Our study showed that TET1, TET2, and TET3 were expressed in NSCs. Addition of VPA to the NSC cultures enhanced TET enzyme activity, and led to a robust increase of global and local 5-hmC in the *Ngn1* gene promoter region as well as in the number of DCX-positive cells. In NSCs cells, a 5-hmC increase was followed by a substantial decrease of 5-mC, indicating that 5-hmC is an intermediate to be eliminated ultimately by the base excision repair pathway. By contrast, the decreases of 5-mC were shown in the VPA-treated NSCs in our study, which is consistent with the previous report of the 5-mC pattern in adult mouse brain (Dong et al., 2010). However, our TET1, TET2, and TET3 knockdown experiments in the presence of VPA revealed an interaction in the opposite direction. These data suggest that 5-hmC may slowly be converted to cytosine during differentiation. This is in agreement with earlier reports on the redundancy and compensatory actions of 5-hmC or TET family proteins (Etchegaray et al., 2015; He et al., 2015) in accounting for global effects. Moreover, we demonstrated that inhibition of PI3K/AKT/mTOR blocks DNA demethylation of *Ngn1* regulatory regions induced by VPA via suppressing TET1, TET2, and TET3, indicating a strong connection between mTOR signaling and TET enzymes during *Ngn1* gene activation.

Epigenetic control of long-distance gene expression by histone modifications is a pivotal mechanism determining cell-fate and cell-phenotype maintenance (Rivera and Ren, 2013). Compared with the generally permissive histone acetylation, histone methylations are more diverse in function and their regulation is complex and dynamic. Methylated histones are associated with promoter activation (H3K4me3) and a repressive heterochromatin structure (H3K9me2, K27me3) (Heintzman et al., 2007; Mosammaparast and Shi, 2010). Enzymes responsible for these modifications are histone methyltransferases and demethylases. We showed that DNA hydroxymethylation promoted by VPA was accompanied with the formation of an open chromatin structure. VPA regulated histone acetylation and methylation, which activates neuron-specific gene expression. Our data showed that VPA exposure caused a reduction in the levels of trimethylated histone H3 on lysine 4 (H3K27 me3), and histone H3-dimethylated lysine 9 (H3K9me2) on the *Ngn1* promoter region accompanies this gene repression in differentiating NSCs. Concomitantly, relatively high levels of the trimethylation of lysine 4 (H3K4 me3) and histone H3-acetylated lysine 9 (H3K9Ac) on the *Ngn1* promoter region were found. These data suggest that the profoundly increased activity of the *Ngn1* gene is associated with transcriptionally active markers (H3K4me3 and H3K9Ac) and two others are associated with repressed markers (H3K9me3 and H3K27me3). A similar conclusion was derived from the observation that the active H3K4me3 and repressive H3K27me3 markers are detected in a large number of developmental regulator genes in mammalian ESCs (Bernstein et al., 2006) and adult stem cells (Cui et al., 2009; Wei et al., 2009). Our present findings also show that mTOR inhibition does not markedly affect the expression of the above H3 modifications during differentiation, indicating that VPA may promote histone modifications through suppressing HDACs activity rather than activating mTOR signaling.

EXPERIMENTAL PROCEDURES

Full experimental procedures are provided in the Supplemental Information.

Cell Culture and Transfection

Hippocampi were dissected from embryonic day 16 (E16) embryos of adult pregnant Sprague-Dawley rats into Hank's balanced salt solution without calcium or magnesium. The dissociated cells were plated on dishes coated with 50 μg/mL poly-L-ornithine and 10 μg/mL fibronectin (Sigma-Aldrich) in N2 medium and incubated at 37°C in a humidified atmosphere of 5% CO_2 and 95% air. Fibroblast growth factor 2 (FGF2, 20 ng/mL, Millipore) was added to expand the population of proliferative progenitors. Cells at 80% confluence were subcultured in N2 medium in the presence of

FGF2 in 24-well plates, and these subcultured cells were used for all experiments. They were induced to differentiate by withdrawing FGF2, and kept in a differentiation medium (neurobasal medium) for 5–7 days with or without VPA, TSA, rapamycin, wortmannin, or AZA. Mouse multipotent C17.2 NSCs were a kind gift from Dr. Weilin Jin (Shanghai Jiao Tong University, China).

Negative control short hairpin RNAs (shRNAs), TET1-, TET2-, TET3-, PI3Kp110α-, and PI3Kp110β-specific shRNA were purchased from Santa Cruz Biotechnology. Recombinant lentiviral vector encoding CA-mTOR activator Rheb (S16H) was purchased from Addgene. Sequences for shRNAs are listed in Table S1.

Immunofluorescence

Cells plated on chamber slides were fixed with 4% paraformaldehyde, permeabilized with 0.2% Triton X-100, and incubated with the primary antibody at 4°C overnight. Chamber slides were subsequently incubated with fluorescein isothiocyanate- or tetramethylrhodamine-conjugated secondary antibody for 1 hr at room temperature. Coverslips were mounted in Gel Mount (VECTASHIELD) and imaged with a Nikon E400 fluorescent microscope (Nikon). The name, catalog numbers, and supplier for antibodies are listed in Table S2.

Statistical Analysis

One-way ANOVA followed by Bonferroni's post hoc test was performed. Student's t test was used for comparisons of two groups. p Values <0.05 were considered significant.

SUPPLEMENTAL INFORMATION

Supplemental Information includes Supplemental Experimental Procedures, one figure, and three tables and can be found with this article online at http://dx.doi.org/10.1016/j.stemcr.2017.04.006.

AUTHOR CONTRIBUTIONS

Conception and Design, A.X., D.L., J.L., and W.J.; Performed Research, X.Z., X.H., Q.L., X.K., Z.O., L.Z., Z.G., and L.X.; Collection and Assembly of Data, M.Z., W.Z., L.Z., and Z.G.; Data Analysis and Interpretation, A.X., L.X., and W.J.; Manuscript Writing, A.X. and M.Z.; Final Approval of Manuscript, all authors.

ACKNOWLEDGMENTS

This work was supported by the National Natural Science Foundation of China (81371217, 81472999, 81473014, 81470205, 81501014), the National Funds of Developing Local Colleges and Universities (B16056001), the Outstanding Young People Project of Guangdong Province (Yq2013137), the Science and Technology Foundation of Guangdong Province (2016A020214019), the Science and Technology Foundation of Guangzhou (201707010231), the Key Natural Science Foundation of Guangdong (2015A030311038), and the Science Foundation of Education Bureau of Guangzhou City (1201610239).

Received: November 5, 2016
Revised: April 4, 2017
Accepted: April 6, 2017
Published: May 9, 2017

REFERENCES

Bernstein, B.E., Mikkelsen, T.S., Xie, X., Kamal, M., Huebert, D.J., Cuff, J., Fry, B., Meissner, A., Wernig, M., Plath, K., et al. (2006). A bivalent chromatin structure marks key developmental genes in embryonic stem cells. Cell *125*, 315–326.

Carabalona, A., Hu, D.J., and Vallee, R.B. (2016). KIF1A inhibition immortalizes brain stem cells but blocks BDNF-mediated neuronal migration. Nat. Neurosci. *19*, 253–262.

Cui, K., Zang, C., Roh, T.Y., Schones, D.E., Childs, R.W., Peng, W., and Zhao, K. (2009). Chromatin signatures in multipotent human hematopoietic stem cells indicate the fate of bivalent genes during differentiation. Cell Stem Cell *4*, 80–93.

Detich, N., Bovenzi, V., and Szyf, M. (2003). Valproate induces replication-independent active DNA demethylation. J. Biol. Chem. *278*, 27586–27592.

Dong, E., Chen, Y., Gavin, D.P., Grayson, D.R., and Guidotti, A. (2010). Valproate induces DNA demethylation in nuclear extracts from adult mouse brain. Epigenetics *5*, 730–735.

Dozawa, M., Kono, H., Sato, Y., Ito, Y., Tanaka, H., and Ohshima, T. (2014). Valproic acid, a histone deacetylase inhibitor, regulates cell proliferation in the adult zebrafish optic tectum. Dev. Dyn. *243*, 1401–1415.

Du, Z., Song, J., Wang, Y., Zhao, Y., Guda, K., Yang, S., Kao, H.Y., Xu, Y., Willis, J., Markowitz, S.D., et al. (2010). DNMT1 stability is regulated by proteins coordinating deubiquitination and acetylation-driven ubiquitination. Sci. Signal. *3*, ra80.

Endo, M., Antonyak, M.A., and Cerione, R.A. (2009). Cdc42-mTOR signaling pathway controls Hes5 and Pax6 expression in retinoic acid-dependent neural differentiation. J. Biol. Chem. *284*, 5107–5118.

Etchegaray, J.P., Chavez, L., Huang, Y., Ross, K.N., Choi, J., Martinez-Pastor, B., Walsh, R.M., Sommer, C.A., Lienhard, M., Gladden, A., et al. (2015). The histone deacetylase SIRT6 controls embryonic stem cell fate via TET-mediated production of 5-hydroxymethylcytosine. Nat. Cell Biol. *17*, 545–557.

Fan, G., Martinowich, K., Chin, M.H., He, F., Fouse, S.D., Hutnick, L., Hattori, D., Ge, W., Shen, Y., Wu, H., et al. (2005). DNA methylation controls the timing of astrogliogenesis through regulation of JAK-STAT signaling. Development *132*, 3345–3356.

Godino, A., Jayanthi, S., and Cadet, J.L. (2015). Epigenetic landscape of amphetamine and methamphetamine addiction in rodents. Epigenetics *10*, 574–580.

Guidotti, A., Auta, J., Chen, Y., Davis, J.M., Dong, E., Gavin, D.P., Grayson, D.R., Matrisciano, F., Pinna, G., Satta, R., et al. (2011). Epigenetic GABAergic targets in schizophrenia and bipolar disorder. Neuropharmacology *60*, 1007–1016.

Gurpur, P.B., Liu, J., Burkin, D.J., and Kaufman, S.J. (2009). Valproic acid activates the PI3K/AKT/mTOR pathway in muscle and ameliorates pathology in a mouse model of Duchenne muscular dystrophy. Am. J. Pathol. *174*, 999–1008.

Hahn, M.A., Qiu, R., Wu, X., Li, A.X., Zhang, H., Wang, J., Jui, J., Jin, S.G., Jiang, Y., Pfeifer, G.P., et al. (2013). Dynamics of 5-hydroxymethylcytosine and chromatin marks in mammalian neurogenesis. Cell Rep. *3*, 291–300.

Han, J., Wang, B., Xiao, Z., Gao, Y., Zhao, Y., Zhang, J., Chen, B., Wang, X., and Dai, J. (2008). Mammalian target of rapamycin (mTOR) is involved in the neuronal differentiation of neural progenitors induced by insulin. Mol. Cell Neurosci. *39*, 118–124.

He, X.B., Kim, M., Kim, S.Y., Yi, S.H., Rhee, Y.H., Kim, T., et al. (2015). Vitamin C facilitates dopamine neuron differentiation in fetal midbrain through TET1- and JMJD3-dependent epigenetic control manner. Stem Cells *33*, 1320–1332.

Heintzman, N.D., Stuart, R.K., Hon, G., Fu, Y., Ching, C.W., Hawkins, R.D., Barrera, L.O., Van Calcar, S., Qu, C., Ching, K.A., et al. (2007). Distinct and predictive chromatin signatures of transcriptional promoters and enhancers in the human genome. Nat. Genet. *39*, 311–318.

Hirabayashi, Y., and Gotoh, Y. (2010). Epigenetic control of neural precursor cell fate during development. Nat. Rev. Neurosci. *11*, 377–388.

Hsieh, J., Nakashima, K., Kuwabara, T., Mejia, E., and Gage, F.H. (2004). Histone deacetylase inhibition-mediated neuronal differentiation of multipotent adult neural progenitor cells. Proc. Natl. Acad. Sci. USA *101*, 16659–16664.

Hu, L., Lu, J., Cheng, J., Rao, Q., Li, Z., Hou, H., Lou, Z., Zhang, L., Li, W., Gong, W., et al. (2015). Structural insight into substrate preference for TET-mediated oxidation. Nature *527*, 118–122.

Kafer, G.R., Li, X., Horii, T., Suetake, I., Tajima, S., Hatada, I., and Carlton, P.M. (2016). 5-Hydroxymethylcytosine marks sites of DNA damage and promotes genome stability. Cell Rep. *14*, 1283–1292.

Kim, M., Park, Y.K., Kang, T.W., Lee, S.H., Rhee, Y.H., Park, J.L., Kim, H.J., Lee, D., Lee, D., Kim, S.Y., et al. (2014). Dynamic changes in DNA methylation and hydroxymethylation when hES cells undergo differentiation toward a neuronal lineage. Hum. Mol. Genet. *23*, 657–667.

Kriaucionis, S., and Heintz, N. (2009). The nuclear DNA base 5-hydroxymethylcytosine is present in Purkinje neurons and the brain. Science *324*, 929–930.

Kundakovic, M., Chen, Y., Guidotti, A., and Grayson, D.R. (2009). The reelin and GAD67 promoters are activated by epigenetic drugs that facilitate the disruption of local repressor complexes. Mol. Pharmacol. *75*, 342–354.

Li, S., Yang, C., Zhang, L., Gao, X., Wang, X., Liu, W., Wang, Y., Jiang, S., Wong, Y.H., Zhang, Y., et al. (2016). Promoting axon regeneration in the adult CNS by modulation of the melanopsin/GPCR signaling. Proc. Natl. Acad. Sci. USA *113*, 1937–1942.

Makarević, J., Tawanaie, N., Juengel, E., Reiter, M., Mani, J., Tsaur, I., Bartsch, G., Haferkamp, A., and Blaheta, R.A. (2014). Cross-communication between histone H3 and H4 acetylation and AKT-mTOR signalling in prostate cancer cells. J. Cell Mol. Med. *18*, 1460–1466.

Marfia, G., Madaschi, L., Marra, F., Menarini, M., Bottai, D., Formenti, A., Bellardita, C., Di Giulio, A.M., Carelli, S., and Gorio, A. (2011). Adult neural precursors isolated from post mortem brain yield mostly neurons: an erythropoietin-dependent process. Neurobiol. Dis. *43*, 86–98.

Martins-Taylor, K., Schroeder, D.I., LaSalle, J.M., Lalande, M., and Xu, R.H. (2012). Role of DNMT3B in the regulation of early neural and neural crest specifiers. Epigenetics *7*, 71–82.

McGann, J.C., Oyer, J.A., Garg, S., Yao, H., Liu, J., Feng, X., Liao, L., Yates, J.R., and Mandel, G. (2014). Polycomb- and REST-associated histone deacetylases are independent pathways toward a mature neuronal phenotype. Elife *3*, e04235.

Mosammaparast, N., and Shi, Y. (2010). Reversal of histone methylation: biochemical and molecular mechanisms of histone demethylases. Annu. Rev. Biochem. *79*, 155–179.

Nicolini, C., Ahn, Y., Michalski, B., Rho, J.M., and Fahnestock, M. (2015). Decreased mTOR signaling pathway in human idiopathic autism and in rats exposed to valproic acid. Acta Neuropathol. Commun. *3*, 3.

Orlanski, S., Labi, V., Reizel, Y., Spiro, A., Lichtenstein, M., Levin-Klein, R., Koralov, S.B., Skversky, Y., Rajewsky, K., Cedar, H., et al. (2016). Tissue-specific DNA demethylation is required for proper B-cell differentiation and function. Proc. Natl. Acad. Sci. USA *113*, 5018–5023.

Otaegi, G., Yusta-Boyo, M.J., Vergaño-Vera, E., Méndez-Gómez, H.R., Carrera, A.C., Abad, J.L., González, M., de la Rosa, E.J., Vicario-Abejón, C., and de Pablo, F. (2006). Modulation of the PI 3-kinase-AKT signalling pathway by IGF-I and PTEN regulates the differentiation of neural stem/precursor cells. J. Cell Sci. *119*, 2739–2748.

Parker, V.E., Knox, R.G., Zhang, Q., Wakelam, M.J., and Semple, R.K. (2015). Phosphoinositide 3-kinase-related overgrowth: cellular phenotype and future therapeutic options. Lancet *385* (*Suppl 1*), S77.

Qiao, Y., Wang, R., Yang, X., Tang, K., and Jing, N. (2015). Dual roles of histone H3 lysine 9 acetylation in human embryonic stem cell pluripotency and neural differentiation. J. Biol. Chem. *290*, 2508–2520.

Qin, L., Dai, X., and Yin, Y. (2016). Valproic acid exposure sequentially activates Wnt and mTOR pathways in rats. Mol. Cell Neurosci. *75*, 27–35.

Rivera, C.M., and Ren, B. (2013). Mapping human epigenomes. Cell *155*, 39–55.

Sun, D.F., Zhang, Y.J., Tian, X.Q., Chen, Y.X., and Fang, J.Y. (2014). Inhibition of mTOR signalling potentiates the effects of trichostatin A in human gastric cancer cell lines by promoting histone acetylation. Cell Biol. Int. *38*, 50–63.

Tan, S.L., Nishi, M., Ohtsuka, T., Matsui, T., Takemoto, K., Kamio-Miura, A., Aburatani, H., Shinkai, Y., and Kageyama, R. (2012). Essential roles of the histone methyltransferase ESET in the epigenetic control of neural progenitor cells during development. Development *139*, 3806–3816.

Teng, H.F., Li, P.N., Hou, D.R., Liu, S.W., Lin, C.T., Loo, M.R., Kao, C.H., Lin, K.H., and Chen, S.L. (2014). Valproic acid enhances Oct4 promoter activity through PI3K/AKT/mTOR pathway activated nuclear receptors. Mol. Cell Endocrinol. *383*, 147–158.

Toma, K., Kumamoto, T., and Hanashima, C. (2014). The timing of upper-layer neurogenesis is conferred by sequential derepression

and negative feedback from deep-layer neurons. J. Neurosci. *34*, 13259–13276.

Wei, G., Wei, L., Zhu, J., Zang, C., Hu-Li, J., Yao, Z., Cui, K., Kanno, Y., Roh, T.Y., Watford, W.T., et al. (2009). Global mapping of H3K4me3 and H3K27me3 reveals specificity and plasticity in lineage fate determination of differentiating CD4+ T cells. Immunity *30*, 155–167.

Wilson-Edell, K.A., Yevtushenko, M.A., Rothschild, D.E., Rogers, A.N., and Benz, C.C. (2014). mTORC1/C2 and pan-HDAC inhibitors synergistically impair breast cancer growth by convergent AKT and polysome inhibiting mechanisms. Breast Cancer Res. Treat. *144*, 287–298.

Wu, H., Coskun, V., Tao, J., Xie, W., Ge, W., Yoshikawa, K., Li, E., Zhang, Y., and Sun, Y.E. (2010). Dnmt3a-dependent nonpromoter DNA methylation facilitates transcription of neurogenic genes. Science *329*, 444–448.

Xia, Q., Zheng, Y., Jiang, W., Huang, Z., Wang, M., Rodriguez, R., and Jin, X. (2016). Valproic acid induces autophagy by suppressing the AKT/mTOR pathway in human prostate cancer cells. Oncol. Lett. *12*, 1826–1832.

Yu, I.T., Park, J.Y., Kim, S.H., Lee, J.S., Kim, Y.S., and Son, H. (2009). Valproic acid promotes neuronal differentiation by induction of proneural factors in association with H4 acetylation. Neuropharmacology *56*, 473–480.

Zhang, R.R., Cui, Q.Y., Murai, K., Lim, Y.C., Smith, Z.D., Jin, S., Ye, P., Rosa, L., Lee, Y.K., Wu, H.P., et al. (2013). Tet1 regulates adult hippocampal neurogenesis and cognition. Cell Stem Cell *13*, 237–245.

Zhao, Z., Fan, L., and Frick, K.M. (2010). Epigenetic alterations regulate estradiol-induced enhancement of memory consolidation. Proc. Natl. Acad. Sci. USA *107*, 5605–5610.

Stem Cell Reports, Volume *8*

Supplemental Information

PI3K/AKT/mTOR Signaling Mediates Valproic Acid-Induced Neuronal Differentiation of Neural Stem Cells through Epigenetic Modifications

Xi Zhang, Xiaosong He, Qingqing Li, Xuejian Kong, Zhenri Ou, Le Zhang, Zhuo Gong, Dahong Long, Jianhua Li, Meng Zhang, Weidong Ji, Wenjuan Zhang, Liping Xu, and Aiguo Xuan

Supplemental Information

PI3K/Akt/mTOR Signaling Mediates Valproic Acid-induced Neuronal Differentiation of Neural Stem Cells through Epigenetic Modifications

Xi Zhang, Xiaosong He, Qingqing Li, Xuejian Kong, Zhenri Ou, Le Zhang, Zhuo Gong, Dahong Long, Jianhua Li, Meng Zhang, Weidong Ji, Wenjuan Zhang, Liping Xu and Aiguo Xuan

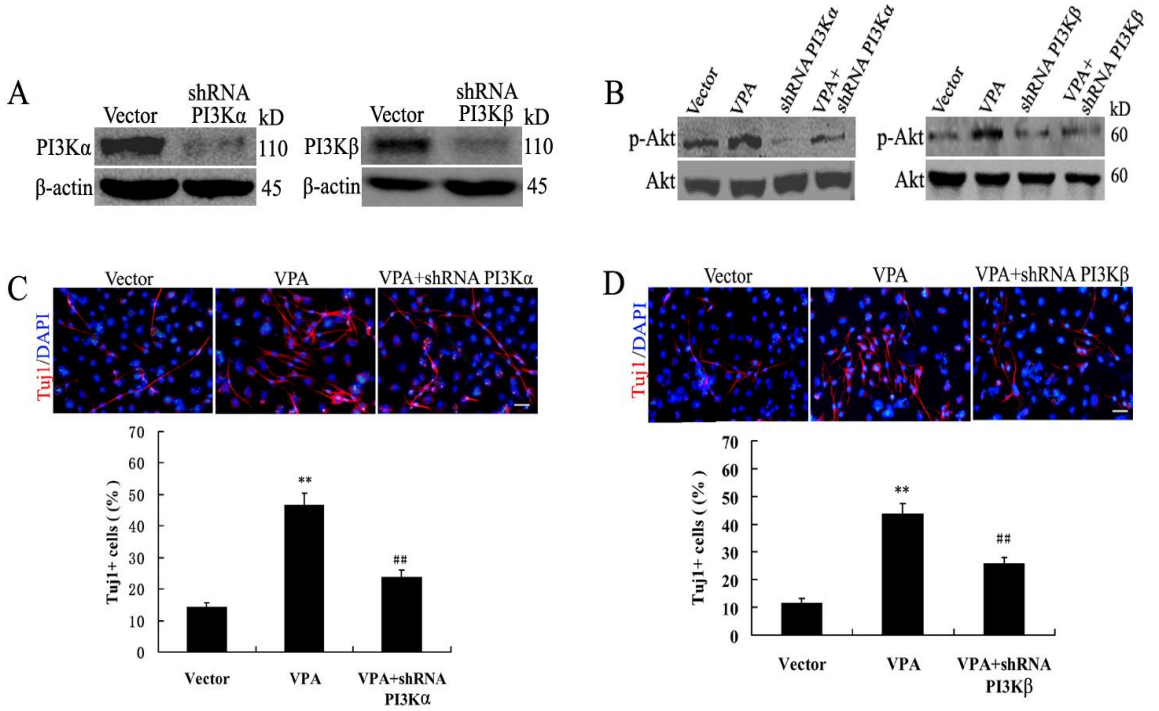

Figure S1

Knocking down PI3K p110α or β expression alleviated the neuronal differentiation of VPA-treated NSCs. Related to Figure 2

(**A**) NSCs were transfected with PI3K p110α or PI3K p110β or control shRNA for 48 h. Lysates from the cells were analyzed by immunoblotting for the levels of PI3K p110α, PI3K p110β and β-actin.

(**B**) PI3K p110α or PI3K p110β knockdown suppressed Akt activation in VPA-treated NSCs.

(**C**) PI3K p110α downregulation reduced the neuronal differentiation of VPA-treated NSCs (scale bar, 100μm). ** $p = 0.000 < 0.01$ compared with control (Vector); $^{\#\#}$ $p = 0.003 < 0.01$ compared with VPA (Vector+VPA).

(**D**) PI3K p110β downregulation decreased the neuronal differentiation of VPA-treated NSCs (scale

bar, 100μm). ** $p = 0.000 < 0.01$ compared with control (Vector); ## $p = 0.004 < 0.01$ compared with VPA (Vector+VPA). All data shown are from three independent experiments.

Table S1

Sequences for shRNAs Related to Figure 7 and Figure S1.

sc-154204-V: Tet1 shRNA (m) Lentiviral Particles is a pool of 3 different shRNA plasmids
sc-154204-VA: Hairpin sequence: GATCCGAAGATGTACCCTCAACAATTCAAGAGATTGTTGAGGGTACATCTTCTTTTT Corresponding siRNA sequences (sc-154204A): • Sense: GAAGAUGUACCCUCAACAAtt • Antisense: UUGUUGAGGGUACAUCUUCtt sc-154204-VB: Hairpin sequence: GATCCCTACCTGTACGTACAGTAATTCAAGAGATTACTGTACGTACAGGTAGTTTTT Corresponding siRNA sequences (sc-154204B): • Sense: CUACCUGUACGUACAGUAAtt • Antisense: UUACUGUACGUACAGGUAGtt sc-154204-VC: Hairpin sequence: GATCCGGAAGCTGTTCGCTAACTATTCAAGAGATAGTTAGCGAACAGCTTCCTTTTT Corresponding siRNA sequences (sc-154204C): • Sense: GGAAGCUGUUCGCUAACUAtt • Antisense: UAGUUAGCGAACAGCUUCCtt Note: all sequences are provided in 5′ → 3′ orientation.
sc-154205-V: Tet2 shRNA (m) Lentiviral Particles is a pool of 3 different shRNA plasmids
sc-154205-VA: Hairpin sequence: GATCCGAGATGCCTTCACTACTAATTCAAGAGATTAGTAGTGAAGGCATCTCTTTTT Corresponding siRNA sequences (sc-154205A): • Sense: GAGAUGCCUUCACUACUAAtt • Antisense: UUAGUAGUGAAGGCAUCUCtt sc-154205-VB: Hairpin sequence: GATCCGGAAGAGTGCGGAAAGAATTTCAAGAGAATTCTTTCCGCACTCTTCCTTTTT Corresponding siRNA sequences (sc-154205B): • Sense: GGAAGAGUGCGGAAAGAAUtt • Antisense: AUUCUUUCCGCACUCUUCCtt sc-154205-VC: Hairpin sequence: GATCCGTTCCTACTTGTCGTCATATTCAAGAGATATGACGACAAGTAGGAACTTTTT Corresponding siRNA sequences (sc-154205C): • Sense: GUUCCUACUUGUCGUCAUAtt

• Antisense: UAUGACGACAAGUAGGAACtt Note: all sequences are provided in 5′ → 3′ orientation.
sc-154206-V: Tet3 shRNA (m) Lentiviral Particles is a pool of 3 different shRNA plasmids
sc-154206-VA: Hairpin sequence: GATCCGGGTTTGTCTATCTCCTTATTCAAGAGATAAGGAGATAGACAAACCCTTTTT Corresponding siRNA sequences (sc-154206A): • Sense: GGGUUUGUCUAUCUCCUUAtt • Antisense: UAAGGAGAUAGACAAACCCtt sc-154206-VB: Hairpin sequence: GATCCCTCTGTGCATTAAGCAGTATTCAAGAGATACTGCTTAATGCACAGAGTTTTT Corresponding siRNA sequences (sc-154206B): • Sense: CUCUGUGCAUUAAGCAGUAtt • Antisense: UACUGCUUAAUGCACAGAGtt sc-154206-VC: Hairpin sequence: GATCCCTGTCTCACAGCATACTAATTCAAGAGATTAGTATGCTGTGAGACAGTTTTT Corresponding siRNA sequences (sc-154206C): • Sense: CUGUCUCACAGCAUACUAAtt • Antisense: UUAGUAUGCUGUGAGACAGtt Note: all sequences are provided in 5′ → 3′ orientation.
sc-39128-V: PI3-kinase p110α shRNA (m) Lentiviral Particles is a pool of 3 different shRNA plasmids
sc-39128-VA: Hairpin sequence: GATCCCACAGACACTACTGCGTAATTCAAGAGATTACGCAGTAGTGTCTGTGTTTTT Corresponding siRNA sequences (sc-39128A): • Sense: CACAGACACUACUGCGUAAtt • Antisense: UUACGCAGUAGUGUCUGUGtt sc-39128-VB: Hairpin sequence: GATCCGAATCCTGCTCACCAACTATTCAAGAGATAGTTGGTGAGCAGGATTCTTTTT Corresponding siRNA sequences (sc-39128B): • Sense: GAAUCCUGCUCACCAACUAtt • Antisense: UAGUUGGUGAGCAGGAUUCtt sc-39128-VC: Hairpin sequence: GATCCGCACAAGAGTACACCAAGATTCAAGAGATCTTGGTGTACTCTTGTGCTTTTT Corresponding siRNA sequences (sc-39128C): • Sense: GCACAAGAGUACACCAAGAtt • Antisense: UCUUGGUGUACUCUUGUGCtt Note: all sequences are provided in 5′ → 3′ orientation.
sc-29447-V: PI3-kinase p110β shRNA (m) Lentiviral Particles is a pool of 4 different shRNA plasmids
sc-29447-VA: Hairpin sequence: GATCCGGAAGCAAGTTCACAACTATTCAAGAGATAGTTGTGAACTTGCTTCCTTTTT

Corresponding siRNA sequences (sc-29447A):
• Sense: GGAAGCAAGUUCACAACUAtt
• Antisense: UAGUUGUGAACUUGCUUCCtt

sc-29447-VB:
Hairpin sequence:
GATCCGAACGACCATATTTGGAATTTCAAGAGAATTCCAAATATGGTCGTTCTTTTT
Corresponding siRNA sequences (sc-29447B):
• Sense: GAACGACCAUAUUUGGAAUtt
• Antisense: AUUCCAAAUAUGGUCGUUCtt

sc-29447-VC:
Hairpin sequence:
GATCCCTACTCTTGTCAATCAAGTTTCAAGAGAACTTGATTGACAAGAGTAGTTTTT
Corresponding siRNA sequences (sc-29447C):
• Sense: CUACUCUUGUCAAUCAAGUtt
• Antisense: ACUUGAUUGACAAGAGUAGtt

sc-29447-VD:
Hairpin sequence:
GATCCCAGACTCGCTGAGAATCTATTCAAGAGATAGATTCTCAGCGAGTCTGTTTTT
Corresponding siRNA sequences (sc-29447D):
• Sense: CAGACUCGCUGAGAAUCUAtt
• Antisense: UAGAUUCUCAGCGAGUCUGtt
Note: all sequences are provided in 5′ → 3′ orientation.

Table S2

Antibodies Related to Figures 1-7 and Figure S1.

Name	Catalogue number	supplier
NeuN	ab104224	Abcam, UK
Doublecortin (DCX)	sc-271390	Santa cruz, USA
GFAP	ab7260	Abcam, UK
beta III Tubulin	ab78078	Abcam, UK
Neurogenin 1(Ngn1)	ab89461	Abcam, UK
Tet1	sc-163443	Santa cruz, USA
Tet2	sc-398535	Santa cruz, USA
Tet3	ABE383	Millipore, USA
5-mC	GTX21884	GeneTex, USA
5-hmC	MABE176	Millipore, USA
p-p70S6K	9204	CST, USA
p70S6K	2708	CST, USA
p-mTOR	2971	CST, USA
mTOR	2972	CST, USA
p-Akt	13038	CST, USA
Akt	9272	CST, USA
Acetyl-H3	7627	CST, USA
H3	14269	CST, USA
Acetyl-H4	2594	CST, USA
H4	2592	CST, USA

Dnmt1	ab13537	Abcam, UK
Dnmt3a	ab2850	Abcam, UK
Dnmt3b	ab79822	Abcam, UK
Dnmt3L	ab3493	Abcam, UK
HDAC1	ab7028	Abcam, UK
HDAC3	ab7030	Abcam, UK
PI3K p110α	4249	CST, USA
PI3K p110β	ab151549	Abcam, UK
H3K4me3	9751	CST, USA
H3K27me3	9733	CST, USA
H3K9me2	4658	CST, USA
H3K9Ac	ab10812	Abcam, UK

Table S3

Primer sequences used for quantitative RT-PCR analysis Related to Figure 3.

Genes	Forword	Reverse	
DNMT1	5′-GGTTCTGCGCGGGGACAGAC-3′	5′-CCGGCAACATGGCCTCAGGG-3′	183bp
DNMT3a	5′-GGTGTGTGTCGAGAAGCTCA-3′	5′-CCAAGGGCCCACTCAATCAT-3′	222bp
DNMT3b	5′-GGGCCGCTACCACGTTCAGG-3′	5′-AGGGCCGTCCTGGCTCAAGT-3′	178bp
DNMT3L	5′-GTATGCCCGGCCTCGCCAAG-3′	5′-CAGGTCCGCGTGCTTGCTCT-3′	208bp
Ngn1	5′-TGTAGCAGTTTGCTGGTCCT-3′	5′-GTAGCTCTGCACGACGATGT-3′	144bp
β-Actin	5′-GCGTCCACCCGCGAGTACAA-3′	5′-ACATGCCGGAGCCGTTGTCG-3′	118bp

Supplemental Experimental Procedures

5-Bromo-2′-deoxyuridine (BrdU) Labeling

Cells in the different treatment groups were incubated in 24-well plates in each group with 10 μg/L BrdU (Sigma-Aldrich) for 24 h. After incubation, the cells were seeded onto 100 μg/mL poly-L-lysine-coated coverslips. An immunocytochemical assay was used to determine the incorporation. Coverslips were mounted with 4′6-diamidino-2-phenylindole (DAPI) was used to counter stain nuclei. Immunoreactive cells were visualized by fluorescence microscopy. Experiments were done by triplicate.

CCK-8 Cell Assay

The CCK-8 assay was used to quantitatively assess cell survival. Briefly, NSCs were seeded in 96-well plates with six replicates in each group, and subjected to the different treatments described. 10 μL CCK-8 solutions were added to each well, and NSCs were incubated for 4 h. The absorbance at 450 nm was measured with a microplate reader (Thermo Fisher Scientific, Japan). Each experiment was repeated for four times.

DNA Methylation and Hydroxymethylation Assay

DNA was prepared using the GeneElute mammalian genomic DNA miniprep kit (Sigma-Aldrich) according to the manufacturer's instructions. DNA quality and concentration was measured by NanoDrop 1000 spectrophotometer (Thermo Scientific). Relative quantitation of *5-mC and 5-hmC* within a specific locus *was performed using* EpiMark™ 5-hmC and 5-mC Analysis Kit (Epigentek, NY) according to the manufacturer's instructions, followed by real-time PCR analysis. The forward and reverse primers for Ngn1 were 5′-TGTAGCAGTTTGCTGGTCCT-3′ and 5′-GTAGCTCTGCACGACGATGT-3′. The PCR cycle conditions were 50 ℃ for 2 min, 95 ℃ for 10 min, 95 ℃ for 15 s, and 60 ℃ for 1 min (40 cycles).

Western Blot

Western blotting was performed as described previously (Xuan et al., 2015). Briefly, cellular proteins were extracted with RIPA lysis buffer containing protease inhibitor cocktail. Protein samples were separated by SDS-PAGE and transferred to polyvinylidene difluoride membranes. Blotting membranes were incubated with 3 % bovine serum albumin in tris buffered saline with tween and probed with corresponding primary antibodies. After incubation with horseradish peroxidasecoupled secondary antibodies for 2 h at room temperature, bands were normalized to β-actin and quantified by densitometry (syngene, UK). The name, catalogue numbers and supplier for antibodies are listed in Supplementary Table 2.

Real Time RT-PCR

Total cellular RNA was extracted using TriZol reagent (Invitrogen) and quantified using the spectrophotometer. Reverse transcription was performed with an ExScript RT Reagent Kit (Takara Bio Inc., China). Real-time PCR analysis was undertaken using SYBR Premix Ex Taq (Takara Bio

Inc., China). The real-time PCR conditions were as follows: initial denaturation at 95 ℃ for 10 s followed by 39 cycles of 95 ℃ for 5 s and 60 ℃ for 20 s. Relative expression for the studied genes was normalized to the mean signals of ß-actin. Primers used are listed in Supplementary Table 3.

Quantitative Chromatin Immunoprecipitation

Chromatin immunoprecipitation (ChIP) experiments were performed with the MAGnify ChIP kit (Life Technologies) according to manufacturer's protocol with the following adjustments. Antibodies against H3K4me3, H3K27me3, H3K9me2, H3K9Ac (all four from Diagenode) and H3 (Abcam) were used. A rabbit IgG (Diagenode) was used as a negative control. Cells were grown in 10-cm dishes, washed with Hank's Balanced Salt Solution (HBSS) and then crosslinked by adding 5 mL of HBSS with 1% formaldehyde for 8 min at room temperature. The crosslinking reaction was stopped by adding 500 μL of 1.25 M glycine and incubating 5 min. Dishes were washed 2 × with 5 mL HBSS and then the cells were scraped from the dishes in two steps using 2.5 mL of HBSS with 2% FBS, 0.1% EDTA and protease inhibitors for each scraping. Chromatin was sheared by sonication in a chilled Bioruptor set to high for 42 cycles of 30 sec on/off. Approximately 200,000 cells were used for each ChIP. Input DNA was purified from a sample aliquot equal to 10% of the total cells used for each ChIP. Equal volumes of ChIP and input DNA were quantified by QRT-PCR using the ABI 7500 Real-Time Detection System. The forward and reverse primers were 5′-TGTAGCAGTTTGCTGGTCCT-3′ and 5′-GTAGCTCTGCACGACGATGT-3′.

5-hydroxymethylated DNA Immunoprecipitation (5hmC DIP)-qPCR and 5-methylated DNA Immunoprecipitation (5mC DIP)-qPCR

Genomic DNA was extracted from cultured cells using the TIANamp Genomic DNA Kit (Tiangen Biotech) according to the manufacturer's instructions and sheared into an average 200–500 bp in length by sonication and immunoprecipitated with a rabbit anti-5hmC polyclonal antibody (Active Motif) and a mouse anti-5mC monoclonal antibody (Gene Tex). 5mC DIP-qPCR and 5hmC DIP-qPCR were performed using the EpiQuik methylated DNA Immunoprecipitation and

EpiQuik methylated DNA Immunoprecipitation Kits (Epigentek) according to the manufacturer's instructions. Immunoprecipitated DNA fragments were collected by magnetic beads, purified, and subjected to real-time qPCR using primers specific to Ngn1 promoter loci (5′-TTACGGGCACGCTCCAGG-3′ and 5′-CCTCAGGACCCCTTAAGTACGG-3′). Data were normalized to values of the input DNA.

DNA Extraction and Bisulfite Sequencing

Genomic DNA was isolated from cultured cells using the DNeasy tissue kit (QIAGEN, Valencia, CA). The extracted DNA was subjected to bisulfite conversion. The bisulfite conversion was carried out using 750 ng of DNA and EZ DNA Methylation Gold Kits (Zymo Research Corp., Orange, CA) following the manufacturer's instructions. The converted DNA was amplified by PCR using Platinum PCR SuperMix (Invitrogen, Carlsbad, CA) with one specific set of primers. One fragment of Ngn1 gene was amplified: fragment included the CpG island from −171 to +140, the forward primer was 5′-GYGAGTATAAATTATGTAAATAGTAGG-3′ and the reverse primer was 5′-CTATACCTACTACAAACRCRAA-3′, PCR amplification conditions were: 94 ℃ 3 min; 94 ℃ 30 s, 60 ℃ 45 s, 72 ℃ 45 s, 35 cycles. The PCR products were cloned into pTG19-T vector using a Generay TA Cloning Kit (Generay Biotech, Shanghai, China). 10 clones from each sample were randomly selected for DNA sequencing using QIAprep Spin Miniprep Kit (QIAGEN, Valencia, CA).

Dot Blot

Total DNA was extracted from cultured cells using the TIANamp Genomic DNA Kit (Tiangen Biotech). DNA was denatured at 99 ℃ and spotted on nylon membrane (Millipore). The membrane was incubated at 80 ℃ for 1 hour for crosslinking and then was blocked with 5% nonfat dry milk (BD Bioscience) dissolved in Phosphate Buffered Saline (PBS) containing 0.05% Tween-20 for 1 hour at RT. Membranes were incubated with primary antibodies against 5-hydroxymethylcytosine (5hmC) (1:1000, Active Motif) or 5-methylcytosine (5mC) (1:1000, Epigentek) at 4 ℃ overnight, followed by incubation with secondary antibodies for 1 hour at RT. Secondary antibodies were donkey anti-rabbit IgG or donkey anti-mouse IgG (1:10000, ABCOM).

Supplemental References

Xuan, A.G., Pan, X.B., Wei, P., Ji, W.D., Zhang, W.J., Liu, J.H., Hong, L.P., Chen, W.L., Long, D.H. (2015). Valproic acid alleviates memory deficits and attenuates amyloid-β deposition in transgenic mouse model of Alzheimer's disease. Mol. Neurobiol. 51, 300-312.